Acta Pharmaceutica Sinica B 2024;14(5):2177−2193

Chinese Pharmaceutical Association
Institute of Materia Medica, Chinese Academy of Medical Sciences

Acta Pharmaceutica Sinica B

www.elsevier.com/locate/apsb
www.sciencedirect.com

ORIGINAL ARTICLE

First total synthesis, antitumor evaluation and target identification of mornaphthoate E: A new tubulin inhibitor template acting on PI3K/Akt signaling pathway

Peipei Shan[a,*,†], Tao Ye[b,†], Ying-De Tang[b,†], Hui Song[b], Chao Wang[b], Kongkai Zhu[c], Feifei Yang[b], Shi-Lei Zhang[d], Pei-Wen Su[b], Shuanhu Gao[e,*], Hua Zhang[b,*]

[a]*Institute of Translational Medicine, the Affiliated Hospital of Qingdao University, College of Medicine, Qingdao University, Qingdao 266021, China*
[b]*School of Biological Science and Technology, University of Jinan, Jinan 250022, China*
[c]*Advanced Medical Research Institute, Cheeloo College of Medicine, Shandong University, Jinan 250012, China*
[d]*College of Pharmaceutical Sciences, Soochow University, Suzhou 215127, China*
[e]*School of Chemistry and Molecular Engineering, East China Normal University, Shanghai 200062, China*

Received 4 October 2023; received in revised form 29 January 2024; accepted 8 February 2024

KEY WORDS

Mornaphthoate E;
Tubulin inhibitor;
Antitumor;
Anti-metastasis;
Breast cancer;
PI3K/Akt

Abstract Mornaphthoate E (MPE) is a prenylated naphthoic acid methyl ester isolated from the roots of a famous Chinese medicinal plant *Morinda officinalis* and shows remarkable cytotoxicity against several human tumor cell lines. In the current project, the first total synthesis of (±)-MPE was achieved in seven steps and 5.6% overall yield. Then the *in vitro* anti-tumor activity of MPE was first assessed for both enantiomers in two breast cancer cells, with the levoisomer exerting slightly better potency. The *in vivo* anti-tumor effect was further verified by applying the racemate in an orthotopic autograft mouse model. Notably, MPE exerted promising anti-metastasis activity both *in vitro* and *in vivo* and showed no obvious toxicity on mice at the therapeutic dosage. Mechanistic investigations demonstrated that MPE acted as a tubulin polymerization stabilizer and disturbed the dynamic equilibrium of microtubules *via* regulating PI3K/Akt signaling. In conclusion, our work has provided a new chemical template for the future design and development of next-generation tubulin-targeting chemotherapies.

*Corresponding authors.
E-mail addresses: peipeishan@qdu.edu.cn (Peipei Shan), shgao@chem.ecnu.edu.cn (Shuanhu Gao), bio_zhangh@ujn.edu.cn (Hua Zhang).
†These authors made equal contributions to this work.

Peer review under the responsibility of Chinese Pharmaceutical Association and Institute of Materia Medica, Chinese Academy of Medical Sciences.

https://doi.org/10.1016/j.apsb.2024.02.012

1. Introduction

Cancer is a multigenic and multicellular disease with uncontrolled growth of cells and poor clinical prognosis[1]. At present, cancer is the 2nd leading cause of human death after cardiovascular diseases[2]. In malignant cases, primary tumors would invade other parts of the body *via* blood circulation, and this process is called cancer metastasis, whereas the prognosis of metastatic cancer is extremely poor. Distant metastasis is usually taken as one of the major factors leading to low survival rate and also the main reason of death[3]. Although great success has been achieved in the prevention and treatment of cancer in the past years, the development of effective therapeutic approaches for preventing cancer recurrence and metastasis remains one of the greatest challenges in medical science.

Microtubule plays important roles in a number of cellular processes comprising cytoskeleton formation and maintenance, the transportation of protein complexes and vesicles, and also the regulation of cell motility, division and apoptosis[4-6]. Because of its pivotal roles in the survival of eukaryotic cells, any interference on microtubule would likely result in cell dysfunction and even death, and it thus has long been regarded as an important target to develop chemotherapeutic agents[7,8]. Microtubule is one of the key components of eukaryotic cytoskeleton and it is dynamically assembled from the heterodimers of α and β-tubulin[9], and the disturbance in microtubule assembly and interference in tubulin polymerization/depolymerization will cause G_2/M phase arrest, eventually leading to cell death[10,11]. During the last several decades, a large number of small-molecule chemicals have been identified as promising microtubule-targeting agents (MTAs)[12], and there have been continuous efforts in the development of new tubulin inhibitors with several candidates (*e.g.*, BNC-105p, CKD-516, CA-4P and AVE8062) being put forward to the clinical trials in recent years[13]. Though tubulin inhibitors are widely used in the clinic for cancer treatment, undesirable side effects and drug resistance due to long-term use still present a big issue[8]. In addition, several first-line tubulin-targeting drugs such as paclitaxel (taxol) are natural molecules with complex structures, and the cost to produce them is still high. Therefore, the discovery and development of new type of tubulin inhibitors still own a place in pharmaceutical industry due to the intrinsic advantages of chemotherapies.

The PI3K/Akt axis is a key signaling pathway in regulating many fundamental biological processes comprising cell migration, proliferation, survival and apoptosis, etc.[14]. Growing evidence has revealed that PI3K/Akt signaling is aberrantly activated in many human cancers[15,16], and it has been recorded to take an essential part in the migration and invasion of cancer by regulating the expression of matrix metalloproteinases[17]. Former studies have also shown that PI3K/Akt signaling participates in the processes of cell apoptosis and migration induced by some MTAs in a variety of cancer cells[18-20]. Meanwhile, this signaling has been found to potentially enhance the stability of microtubules thus promoting the invasion and migration process of tumor cells[21]. These findings readily lead to the hypothesis that targeting PI3K/Akt signaling may impair microtubule network, and this pathway may play an important role in the anticancer activity of MTAs.

Previously from *Morinda officinalis*, we separated and identified a pair of naphthoate enantiomers, (+)/(−)-mornaphthoate E (MPE), which showed significant cytostatic activity against human lung (A549) and breast (MCF-7 & MDA-MB231) cancer cells[22]. However, no further antitumor evaluation was performed on the two enantiomers due to their low natural abundance. In this study, the biomimetic total synthesis of (±)-MPE was accomplished for the first time, which provided extra sample supply to support the subsequent biological studies. In general, (+)/(−)-MPE significantly inhibited the proliferation, migration and invasion, as well as halted the cycle progression at G_2/M phase, of MDA-MB231 and MCF-7 cells. Mechanistic investigations unveiled (+)/(−)-MPE as tubulin polymerization stabilizers that disturbed the dynamic equilibrium of microtubule assembly and resulted in the damage to microtubule network, and this could be achieved by regulating PI3K/Akt signaling. Lastly, while showing no obvious toxicity on the tested mice, (±)-MPE strongly prevented the tumor metastasis from breast to lung and other organs in an experimental metastasis mouse model. Details of the synthesis, antitumor evaluation and target identification for MPE will be presented below.

2. Results

2.1. Chemistry

The structure of MPE (**1**) is shown in Scheme 1. It contains a 1,4-naphthoquinone-based tetracyclic ring system incorporating a novel dioxabicyclo[3.2.1]oct-2-ene motif, and the challenge for its total synthesis could be the construction of the seven-membered ring. From our retrosynthetic analysis (Scheme 1), we envisioned solving the potential issues in the assembly of the cycloheptene ring by olefin cross-metathesis and pericyclic reactions. Firstly, MPE (**1**) could be obtained from its cometabolite nonin A

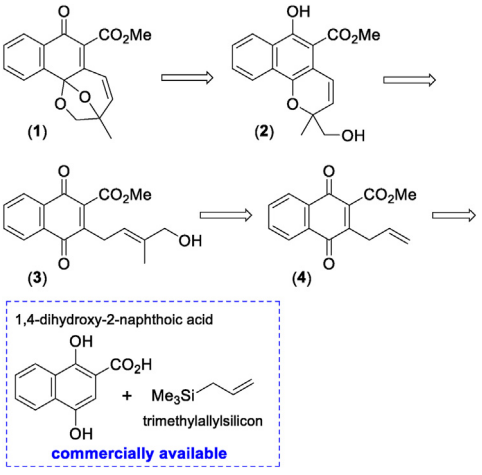

Scheme 1 Retrosynthetic analysis of MPE.

(**2**), which may also be a likely biosynthetic precursor of the former, *via* oxidative ring closing reaction, and the latter could be synthesized from **3** *via* 6π electrocyclic reaction under basic condition. Then the key intermediate **3** can be acquired by the metathesis reaction of methallyl alcohol with 3-allyl-2-methoxycarbonyl-1,4-naphthoquinone (**4**) which could be readily synthesized from commercially available cheap reagents.

The whole synthesis (Scheme 2) started from the commercial product 1,4-dihydroxy-2-naphthoic acid (**5**) which was methylated by iodomethane to afford the corresponding methyl ester (**6**, 97.5% yield), and the latter was transformed to its naphthoquinone form (**7**, 97.9% yield) *via* oxidation. The tried oxidants included (diacetoxyiodo)benzene, DDQ (2,3-dichloro-5,6-dicyano-1,4-benzoquinone) and silver oxide, and Ag_2O with diethyl ether as solvent was eventually chosen based on an overall consideration of yield and post-reaction workup.

Next, the allylation at C-3 of **7** was attempted. Kimpe et al. once reported similar reaction of tributylprenyltin with **7**[23], but considering the toxicity of tin reagents, we selected trimethylallylsilicon (TMAS) for reaction exploration. Interestingly, compound **6** and its 3-allyl derivative (**4a**) were also obtained (Supporting Information Scheme S1). We assumed that the byproduct **4a** could be oxidized by **7** (as a weak oxidant) to the target molecule **4** and compound **7** itself was reduced back to **6**, and this was further confirmed by the reduction of mixture **4/4a** (by sodium hydrosulfite) to pure **4a** and the oxidation of **4/4a** (by DDQ) to pure **4** during the further optimization process. Thus in the following scale-up reaction for sample accumulation, **4** and **4a** were isolated together and then oxidized to pure **4** (42.4% yield) by DDQ for subsequent work. Other ring-closing byproducts were also detected (Scheme S1). Compared with that by Kimpe and co-workers[23], our reaction using TMAS afforded similar products with less allylation products but more cyclization byproducts. In addition, TMAS is more environmentally friendly than the tin reagent.

After the synthesis of **4**, the olefin cross-metathesis reaction[24] was employed to acquire the key intermediate (**3**). The reaction of **4** with methallyl alcohol proved unsuccessful by using the 1st generation Grubbs catalyst. Then the 2nd generation Hoveyda-Grubbs catalyst was applied and different temperatures and reacting times were screened (Supporting Information Table S1). Compound **3** was finally obtained in 24.8% yield at 80 °C in toluene with an 8-h reaction time. It is worth noting that when the reaction continued for longer time (overnight), the next-step product **2** was also detected.

Lastly, the natural cometabolite nonin A (**2**, 76.6% yield) of MPE (**1**) was obtained from **3** *via* a pericyclic oxa-6π ring-closing reaction in the presence of Et_3N, and nonin A (**2**) was further oxidized by (diacetoxyiodo)benzene to afford the final product MPE (**1**, 72.8% yield) as a racemate. The racemic MPE (**1**) was then fractionated on a chiral column to afford the pure enantiomers (+)/(−)-MPE (Supporting Information Fig. S22) for further studies. As the two enantiomers exhibited activity difference at cell level[22], their subsequent *in vitro* antitumor effects were evaluated separately.

2.2. Biology

2.2.1. (+)/(−)-MPE inhibit the proliferation of MDA-MB231 and MCF-7 cells

To examine the antiproliferative effect of (+)/(−)-MPE, we performed MTT assay using MDA-MB231 and MCF-7 cells. As shown in Fig. 1A and B, both enantiomers effectively suppressed the viability of the two cancer cells in a dose-dependent manner. To fully assess the cytostatic effect of (+)/(−)-MPE, cell viability was further detected after 24, 48 and 72 h treatment by the two compounds. The data in Fig. 1C and D and Supporting Information Table S2 revealed that the two enantiomers could decrease the tumor cell proliferation in a time-dependent way. Colony formation is believed to well simulate the pathological process of tumor progression *in vivo*. We then analyzed the clonogenicity of MDA-MB231 and MCF-7 cells upon (+)/(−)-MPE treatment. As shown in Fig. 1E and F, they remarkably inhibited the colony formation of tumor cells in a concentration-dependent manner. In addition, the expression level of proliferating cell nuclear antigen (PCNA) was obviously decreased by treatment of the

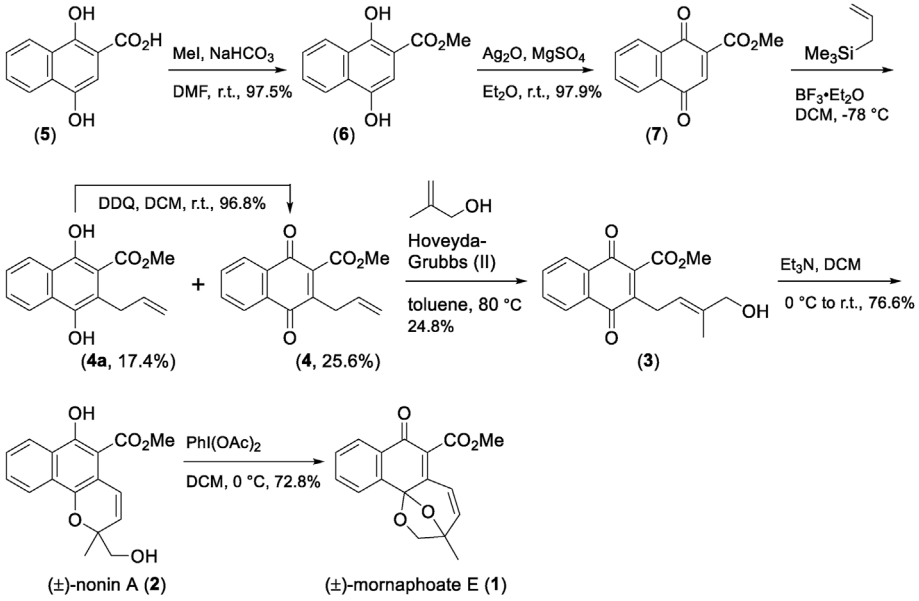

Scheme 2 Total synthesis of MPE.

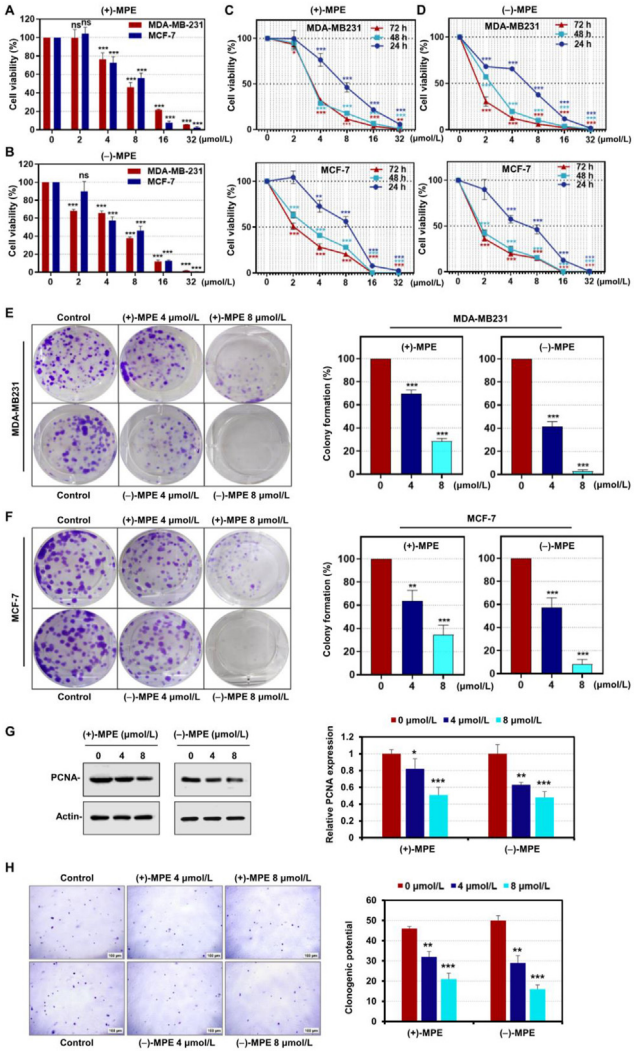

Figure 1 (+)/(−)-MPE prevent the proliferation of MDA-MB231 and MCF-7 cells. (A, B) MDA-MB231 and MCF-7 cells were treated with increasing concentrations of (+)/(−)-MPE, and MTT assay was performed after 24 h. The bars indicate mean ± SD (n = 3). (C, D) MDA-MB231 and MCF-7 cells were treated with increasing concentrations of (+)/(−)-MPE for 24, 48 and 72 h, respectively, and MTT assay was conducted. The bars represent mean ± SD (n = 3). (E, F) MDA-MB231 and MCF-7 cells were seeded in 6-well plates. After 12 h, cells were treated with indicated concentrations of (+)/(−)-MPE. On the 10th day, the number of colonies were counted. Bars represent mean ± SD of three independent experiments. (G) MDA-MB231 cells were treated with increasing concentrations of (+)/(−)-MPE and the expression of PCNA was detected by immunoblotting assay. Protein expressions were quantitated by densitometry and normalized against that of β-actin. Bars represent mean ± SD from three independent experiments. (H) MDA-MB231 cells were treated with increasing concentrations of (+)/(−)-MPE, and then soft agar colony formation assay was performed. The bars indicate mean ± SD (n = 3). ns, no significant difference, *P < 0.05, **P < 0.01, ***P < 0.001 *versus* the control group.

two enantiomers according to Western blot experiment (Fig. 1G). Moreover, we also performed soft agar colony formation assay, and it is clearly shown by the representative pictures and cartograms in Fig. 1H that both cell volume and count were impaired by incubation with (+)/(−)-MPE. These results suggest that both (+) and (−)-MPE show promising antiproliferative activity toward the tested cancer cells *in vitro*.

2.2.2. (+)/(−)-MPE block the migration and invasion of MDA-MB231 and MCF-7 cells

Tumor metastasis requires precise regulation of various cellular processes, including cell migration and invasion, and inhibiting the two important cellular events is an effective strategy to suppress tumor development. Thus the anti-migration and anti-invasion effects of (+)/(−)-MPE against MDA-MB231 and MCF-7 cells were then detected by Wound-healing and Transwell assays *in vitro*. The photographs and statistical data in Fig. 2A−C clearly showed that the wound healing rates of the two cells were remarkably restrained by co-incubation with the two compounds. Moreover, representative images and cell counts from Transwell assay revealed that the invasion of MDA-MB231 and MCF-7 cells were markedly blocked by (+)/(−)-MPE treatment (Fig. 2D and E). Epithelial-mesenchymal transition (EMT) is considered as a key mechanism for regulating the initial steps of metastatic progression[25], and the expression of EMT-associated marker proteins was then detected after administration of the two enantiomers. Fig. 2F illustrated that (+)/(−)-MPE could remarkably upregulate the expression level of epithelial cell marker E-cadherin while downregulate that of mesenchymal markers ZEB1 (zinc-finger E-box binding homeobox 1) and vimentin. Together, these observations indicate that both (+) and (−)-MPE possess potent tumor metastasis inhibitory effects *in vitro*.

2.2.3. (+)/(−)-MPE induce apoptosis and cycle arrest in MDA-MB231 and MCF-7 cells

Induction of apoptosis and cycle arrest represents two major approaches by which most clinical chemotherapies kill tumor cells. Flow cytomertic analyses were thereby conducted to examine whether (+)/(−)-MPE induced the apoptosis and cycle arrest in MDA-MB231 and MCF-7 cells. The results of Annexin V-FITC/PI analysis in Fig. 3A−C demonstrated that both enantiomers significantly increased the percentage of apoptotic cells. Meanwhile, Western blot experiments revealed that the expression level of cleaved PARP and cleaved caspase-3, which are biomarkers of apoptosis, steadily enhanced upon administration of increasing concentrations of (+)/(−)-MPE (Fig. 3D). Next, the cell cycle distributions of MDA-MB231 and MCF-7 after exposure to (+)/(−)-MPE were examined. As shown in Fig. 3E and F, the two enantiomers induced remarkable G_2/M phase arrest in the two cell lines. Additionally, we performed Western blotting assay to evaluate the expression level of cell cycle related proteins (Cdc25c, CDK1, and Cyclin B1) after (+)/(−)-MPE treatment. As shown in Fig. 3G and H, both compounds indeed diminished the expression of Cdc25c and CDK1 while increased that of Cyclin B1 at protein level.

2.2.4. (+)/(−)-MPE inhibit the depolymerization of tubulin

As is known to all, β-tubulin is widely used as an internal reference in Western blot analyses owing to that it is constantly expressed in the growth stage of cells and its content is relatively stable. However, during the detection of the above-mentioned proteins with β-tubulin as the reference, the expression of the latter was also remarkably altered. Also, considering that many natural MTAs, such as taxol, colchicine and vincristine, all cause severe G_2/M phase arrest, it is thus speculated that (+)/(−)-MPE

may also act on microtubules. Then Western blotting experiment was first performed to detect the influence of the two enantiomers on α/β-tubulin. As shown in Fig. 4A and B, the expressions of the two tubulin subunits, particularly that of β-tubulin, were both obviously downregulated compared with the blank control. To further confirm how (+)/(−)-MPE impact and act on the tubulin protein, an *in vitro* tubulin polymerization assay was then conducted with taxol (tubulin polymerization stabilizer) and colchicine (tubulin depolymerization inducer) as reference drugs. The tubulin polymerization curves in Fig. 4C and D clearly revealed that both compounds promoted the polymerization of tubulin in a concentration-relying mode, indicating their nature as tubulin depolymerization inhibitors (or polymerization stabilizers). Moreover, cellular thermal shift assay (CESTA), which is based on the biophysical principle of ligand-induced thermal stabilization of target proteins, was then conducted in MDA-MB231 cells to verify the interaction of (+)/(−)-MPE with tubulin. The immunoblotting analytical results in Fig. 4E indicated that both enantiomers could bind to β-tubulin and stabilize the protein in intact cells.

To further explore the possible binding site(s) of (+)/(−)-MPE to tubulin, molecular docking experiment was conducted. There have been seven binding sites of tubulin inhibitors reported to date[26,27], and interestingly the two tubulin stabilizer binding sites had both been first reported and named after natural product molecules, *i.e.,* taxane site and laulimalide site. Therefore, (+)/(−)-MPE were docked into the two binding sites, and as shown in Fig. 4F and Supporting Information Fig. S23, both enantiomers displayed obviously superior docking scores with laulimalide site than with taxane site, implying that they could bind to the former. The detailed interactions of the two enantiomers with the laulimalide site were visualized in Supporting Information Fig. S24, revealing that (−)-MPE showed one more polar and one more charged interactions than (+)-MPE with the protein. Therefore, this docking work supported the stronger binding affinity of the (−)-enantiomer than the (+)-enantiomer to tubulin, which was well in accord with the cell-level activity.

2.2.5. *(+)/(−)-MPE induce cell death by disrupting the dynamic equilibrium of tubulin assembly*

To further check the impact of (+)/(−)-MPE on microtubules in living cells, a series of experiments were then carried out. Immunofluorescence assay was first conduced to examine the integrity and structure change of microtubules after treatment of the two enantiomers. Fig. 5A and B illustrated that normal MDA-MB231 cells in the control group displayed well-organized microtubule networks which extended throughout the whole cell to maintain the cell morphology, while treatment with (+)/(−)-MPE led to disordered and reduced microtubule networks, as well as cell shrinkage. We next detected whether the two compounds influenced the stability of microtubules by analyzing the expression of acetyl-α-tubulin (Ac-α-tubulin) which had been reported to be an indicator of microtubule stability[28]. The immunofluorescence pictures in Fig. 5C revealed that the expression of Ac-α-tubulin was remarkably downregulated by (+)/(−)-MPE treatment in a concentration-dependent manner. Lastly, microtubules are well known to be one of the main components of cytoskeleton, so the cell morphological change upon treatment of (+)/(−)-MPE was further observed. The photographs in Fig. 5D and E showed that both MDA-MB231 and MCF-7 cells became round after exposure to the two samples, and as the doses increased (4, 8 and 12 μmol/L), all tumor cells shrank and eventually died (cell numbers in the visual field markedly deceased). Together, these results demonstrate that (+)/(−)-MPE could induce cell death by disrupting the dynamic equilibrium of tubulin assembly.

2.2.6. *(+)/(−)-MPE regulate microtubule stability via inhibiting PI3K/Akt signaling pathway*

Former studies had reported that MTAs induced apoptosis *via* regulating PI3K/Akt signaling in a variety of cancer cells[18,19]. It is a well-accepted fact that the apoptosis mechanism is microtubule-dependent and incorporates the PI3K/Akt signaling process, and activating this signaling pathway has proven to potentially enhance the stability of microtubules[20,21]. To delve into the effects of (+)/(−)-MPE on this signaling, the protein levels, both overall and phosphorylated, of PI3K and Akt in MDA-MB231 cells were evaluated. As illustrated in Fig. 6A, a significant concentration-dependent decline of the expression of p-PI3K and p-Akt was observed, while the aggregate levels of PI3K and Akt remained stable. Additionally, through an immunofluorescence analysis, it was confirmed that both enantiomers consistently lowered the p-Akt expression as the dose increased (Fig. 6B). Collectively, these results reinforce the notion that (+)/(−)-MPE may undermine microtubule stability by targeting the PI3K/Akt pathway.

2.2.7. *(±)-MPE inhibits tumor growth and metastasis in a preclinical animal model*

Given that the cytostatic activity of (±)-MPE fell in the middle range of those of (+)/(−)-MPE (Supporting Information Fig. S25) with no antagonistic or synergistic effect, and that the two enantiomers exerted close *in vitro* anti-tumor activity, the subsequent *in vivo* evaluation was then carried out by using the racemate in an orthotopic autograft mouse model. 4T1 cells encoding a luciferase reporter gene were subcutaneously introduced into the 4th abdominal mammary fat pad of female BALB/c mice. After a week, these mice were administered with either (±)-MPE (5 mg/kg) or PBS every other day for a month. Fig. 7A−C show cases that (±)-MPE treatment considerably suppressed tumor progression, leading to significant reductions in both tumor size and weight compared with those of the control group. Examination of the harvested tumor tissues also revealed reduced tumor proliferation due to treatment of (±)-MPE, as evaluated *via* anti-Ki67 and anti-PCNA staining by histological analysis (Fig. 7D). Consistent with the *in vitro* results, (±)-MPE treatment significantly prevented the tumor metastasis from breast to lung (Fig. 7E and F). Next, the primary organs from all mice were extracted and imaged for detection of tumor presence. As can be seen from Fig. 7G and H, only one mouse treated with (±)-MPE had significant lung metastasis, with no other remote metastatic sites being observed. Conversely, tumors in the non-treated mice advanced aggressively, with all the five experiencing severe metastases in various organs: lung (n = 5), liver (n = 4), kidneys (n = 3), and spleen (n = 2). In addition, we also photographed and examined the microtubule networks in the tumor tissues (Fig. 7I), and in agreement with the *in vitro* data, treatment with (±)-MPE disturbed the expression and assembly of tubulin. Moreover, immunoblotting experiment verified the downregulation of β-tubulin in the tumor tissues of (±)-MPE-administrated group compared with the contorl group (Fig. 7J). Notably, the decreased p-PI3K and p-Akt levels in the primary tumor tissues of drug-treated group confirmed the inhibition of (±)-MPE on PI3K/Akt signaling *in vivo* (Fig. 7K), which

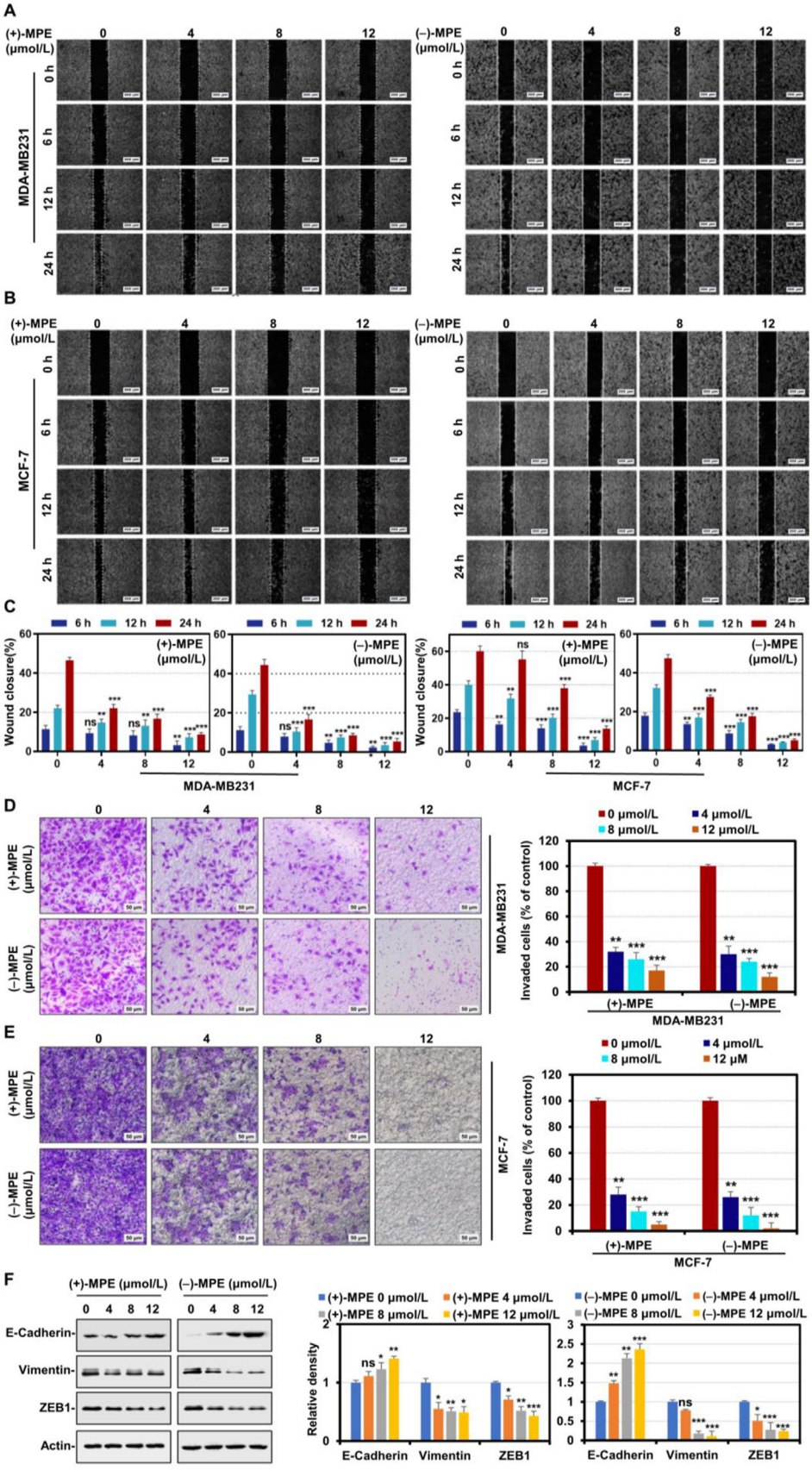

Figure 2 (+)/(−)-MPE inhibit the migration and invasion of breast cancer cells. (A–C) MDA-MB231 and MCF-7 cells in 6-well plates were scratched to create a wound and starved in serum-free medium overnight followed by exposure to different concentrations of (+)/(−)-MPE. Images

supported the notion that the *in vivo* inhibitory effects of (±)-MPE on tumor growth and metastasis could also be linked to the suppression of the PI3K/Akt signaling.

2.2.8. *(±)-MPE shows no systematic toxicity on mice*

To evaluate the potential adverse effects of (±)-MPE *in vivo*, female BALB/c mice were treated with either PBS or (±)-MPE (5 mg/kg) for a duration of 28 days. Body weight was subsequently monitored weekly, and at the conclusion of the study, organ weights were also measured. Encouragingly, mice treated with (±)-MPE showed no discernible reduction in either overall body or primary organ weights (Fig. 8A and B). In addition, histological analysis revealed that (±)-MPE treatment showed no obvious impairment to all major organs (heart, liver, spleen, lung and kidney) of the tested mice compared with the control group (Fig. 8C). Importantly, parameters such as alanine aminotransferase (ALT) and aspartate aminotransferase (AST) levels are recognized indicators of liver health, and blood urea nitrogen (BUN) provides insight into the well-being of kidney and liver. We then detected the post-experiment levels of ALT, BUN and AST in mice treated with (±)-MPE. The data from Fig. 8D revealed no significant alterations in these parameters when the mice were administered with the specified dosage of (±)-MPE. In summary, these observations highlight that (±)-MPE administration did not produce any widespread toxic effects in the experimental mice.

2.2.9. *Evaluation of preliminary pharmacokinetics and bioavailability data of (±)-MPE*

Lastly, in order to provide further guide for the future design and development of better candidate molecules, a preliminary investigation on the pharmacokinetics and bioavailability of (±)-MPE was conducted. As shown in the Supporting Information pharmacokinetics experimental report, (±)-MPE showed decent oral bioavailability (28.04%) but relatively short elimination half-life (0.391 and 0.839 h for iv and *po* administrations, respectively. These data suggest that (±)-MPE may have good permeability in the gastrointestinal tract but relatively poor metabolic stability *in vivo*, which provides a direction for the next-step structural modification and optimization.

3. Discussion and conclusions

It has long been known since the 1960s that a pair of enantiomers can exert different degrees of bioactive potency or even totally different biological properties[36]. However, the rule or regularity of why and how the two enantiomers show bioactivity difference is very complicated and remain a puzzle to be explored. In the current work, we have discovered that both levoisomer and dextroisomer of MPE exhibited *in vitro* antitumor effect, with the (−)-enantiomer displaying mildly higher potency. In addition, the cytostatic effect of the racemate (±)-MPE only showed a simple superimposition of that of (+)/(−)-MPE (Fig. S25), and further assessment of (±)-MPE in animal experiment confirmed its *in vivo* antitumor activity as a racemate, which to a certain degree could be an advantage in that the cost for further racemate-based drug development will be much lower than that for pure enantiomers.

Currently, most chemotherapies for cancer treatment aim to eradicate cancer cells, and this heavily depends on their genotoxic/cytotoxic capability. However, these external stimuli also entice tumor to develop the ability of drug resistance by circumventing the death programs, finally leading to clinical relapse and metastasis[37]. Therefore, targeting tumor metastasis is also an important approach in cancer prevention, apart from killing cancer cells. Tumor metastasis is known as a progressive process involving the formation and colonization of metastatic lesions. The present work revealed that MPE impeded the migration and invasion of MCF-7 and MDA-MB231 cells, and blocked the metastasis of breast cancer to lung and other organs in an experimental metastasis mouse model, which supported the inhibitory capability of MPE toward metastasis formation. It has been known that the dynamic equilibrium of microtubules is indispensable for the polarization and migration of many types of cells and its regulation is critical to the understanding of the molecular basis of cell migration[38]. There is also work reporting that the PI3K/Akt signaling plays a role in the microtubule stabilization of migrating fibroblasts[21]. Our current study has disclosed that MPE could disturb the dynamic equilibrium and impair the network of microtubules *via* regulating PI3K/Akt signaling in cancer cells. However, the detailed mechanism how MPE regulates the microtubule dynamics *via* PI3K/Akt signaling requires further investigation.

Tubulin has been regarded as one of the most successful molecular targets in antitumor drug discovery[39,40], and at present, vinblastine, taxane and colchicine sites are the mostly studied binding sites in the research of new tubulin inhibitors[41]. MTAs with good antitumor activity, such as taxol (paclitaxel), vinblastine and vincristine, have been successfully applied in the clinic for cancer treatment for a long time[42]. However, they still cannot fully satisfy our increasing demand for better therapies due to deficiencies like poor bioavailability, drug resistance and side effects[43-45]. Therefore, the discovery and development of new-generation tubulin inhibitors have always been on the way. In the present work, we have identified MPE as a new type of tubulin inhibitor that act as tubulin polymerization stabilizer likely binding to the laulimalide site, which provides a new template structure for further design of more promising candidate molecules.

To summarize, herein we report the total synthesis of (±)-MPE in detail for the first time and unveil it as a new MTA with promising anticancer effect both *in vitro* and *in vivo*. Particularly, MPE shows strong anti-metastasis activity with no obvious toxicity on the experimental animal at the therapeutic dosage. Mechanistically, MPE could promote the polymerization of tubulin and impair the network of microtubules likely *via* regulating PI3K/Akt signaling pathway. Overall, this work has

were taken after 6, 12 and 24 h of incubation at 37 °C. Bars represent mean ± SD of three independent experiments. (D, E) MDA-MB231 and MCF-7 cells (1×10^5) were re-suspended in serum-free medium and seeded into the upper side of the transwell insert pre-coated with Matrigel. Increasing concentrations of (+)/(−)-MPE were added to both chambers. Images were obtained after 12 h of incubation. Bars represent mean ± SD of three independent experiments. (F) MDA-MB231 cells were treated with indicated concentrations of (+)/(−)-MPE and the expressions of EMT-relevant proteins were detected by Western blotting assay with the indicated antibodies. Protein expressions were quantitated by densitometry and normalized against that of β-actin. Bars represent mean ± SD of three independent experiments. ns, no significant difference, $^*P < 0.05$, $^{**}P < 0.01$, $^{***}P < 0.001$ *versus* the control group.

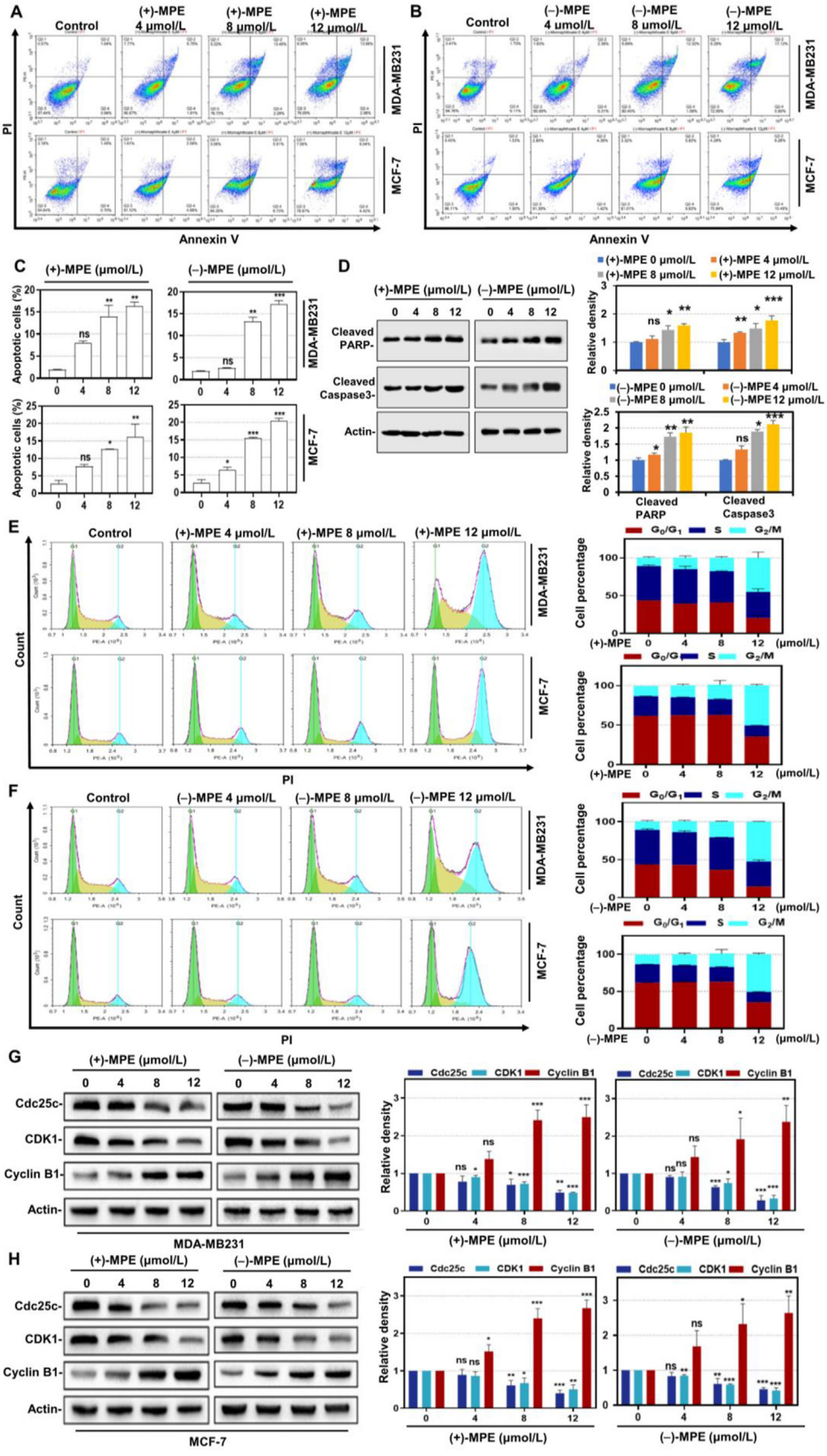

Figure 3 (+)/(−)-MPE induce apoptosis and cycle arrest in MDA-MB231 and MCF-7 cells. (A–C) MDA-MB231 and MCF-7 cells were left untreated or treated with (+)/(−)-MPE at the indicated doses for 24 h. Apoptotic cells were labelled with Annexin V and PI and analyzed by flow

presented evidence that MPE could serve as a new lead molecule for the future development of more tubulin-targeting chemotherapies for cancer treatment.

4. Experimental

4.1. Chemistry

4.1.1. General experimental procedures

See Supporting Information.

4.1.2. Syntheses

*Methyl 1,4-dihydroxy-2-naphthoate (**6**).* The starting compound **5** (204.0 mg, 1.0 mmol, 1.0 equiv.) was dissolved in 10 mL DMF at r.t. and $NaHCO_3$ (168.0 mg, 2.0 mmol, 2.0 equiv.) was then added to the solution. This mixture was stirred for 30 min before the adding of CH_3I (74.7 μL, 1.2 mmol, 1.2 equiv.), and the reaction was monitored by TLC until the end. The final reaction mixture was diluted with water (10 mL) and then partitioned with CH_2Cl_2 (3 × 10 mL). The organic phase was combined, rinsed with saturated NaCl (3 × 10 mL) and dried over Na_2SO_4. The acquired filtrate was solvent-removed *in vacuum* and finally separated on silica gel column (light petroleum/EtOAc, 100:1 to 20:1) to afford **6** (212.7 mg, 97.5% yield). ^{1}H NMR (500 MHz, DMSO-d_6) δ 11.31 (brs), 9.93 (brs), 8.26−8.22 (m), 8.13−8.09 (m), 7.69−7.64 (m), 7.62−7.57 (m), 7.09 (s), 3.93 (s, 3H) ppm. ^{13}C NMR (125 MHz, DMSO-d_6) δ 170.7, 152.8, 145.2, 129.2, 128.9, 126.6, 125.0, 123.3, 122.3, 104.9, 103.9, 52.7 ppm.

*2-Methoxycarbonyl-1,4-naphthoquinone (**7**).* The methyl naphthoate **6** (109.0 mg, 0.50 mmol, 1.0 equiv.) was dissolved in 10 mL Et_2O at r.t. and Ag_2O (381 mg, 1.64 mmol, 3.3 equiv.) and $MgSO_4$ (120 mg, 1.0 mmol, 2.0 equiv.) were then added to the solution. This reaction mixture was retained at r.t. for 16 h followed by filtration with celite (diatomaceous earth). The obtained filtrate was rinsed with ice-cold Et_2O (3 × 10 mL) and condensed *in vacuo* to yield **7** (105.8 mg, 97.9% yield). ^{1}H NMR (600 MHz, chloroform-*d*) δ 8.16−8.12 (m), 8.10−8.06 (m), 7.83−7.76 (m, 2H), 7.27 (d, J = 1.0 Hz), 3.95 (s, 3H) ppm. ^{13}C NMR (150 MHz, chloroform-*d*) δ 184.7, 181.3, 163.9, 139.6, 138.5, 134.7, 134.4, 131.9, 131.7, 127.2, 126.5, 53.3 ppm.

*3-Allyl-2-methoxycarbonyl-1,4-naphthoquinone (**4**).* Under the protection of nitrogen gas, the solution of intermediate **7** (100.0 mg, 0.46 mmol, 1.0 equiv.) in 10 mL dichloromethane was slowly added $BF_3{\cdot}Et_2O$ (63 μL, 0.51 mmol, 1.1 equiv.) at −78 °C. Twenty min later, allyltrimethylsilane (66 μL, 0.42 mmol, 0.9 equiv.) was supplemented to the reaction mixture and the stirring continued for another 4 h at −78 °C until the finish. The reaction was stopped by water (10 mL) followed by removal of the organic phase, and the raw product was recovered from the water phase by partition with dichloromethane (3 × 10 mL). The organic partition phase was combined, rinsed with NaCl solution (10 mL), dried over Na_2SO_4, filtered, solvent-removed and finally purified on silica gel column (light petroleum ether/EtOAc, 100:1 to 20:1) to afford **4** (30.2 mg, 25.6% yield). ^{1}H NMR (500 MHz, chloroform-*d*) δ 8.14−8.07 (m, 2H), 7.80−7.75 (m, 2H), 5.88−5.80 (m), 5.19 (dd, J = 17.1, 1.5 Hz), 5.12 (dd, J = 10.0, 1.3 Hz), 3.95 (s, 3H), 3.34 (dt, J = 6.7, 1.4 Hz, 2H) ppm. ^{13}C NMR (125 MHz, chloroform-*d*) δ 184.2, 182.0, 164.9, 145.0, 139.6, 134.4, 134.4, 132.8, 131.8, 131.5, 126.9, 126.6, 118.6, 52.9, 32.2 ppm.

DDQ (26.5 mg, 0.117 mmol, 1.5 equiv.) was added to the solution of **4a** (20.0 mg, 0.077 mmol, 1.0 equiv.) in 10 mL dichloromethane at r.t. This reaction solution was stirred for an h until the end and then quenched by 5% $NaHCO_3$ (5 mL), followed by removal of the organic phase. The water phase was partitioned with dichloromethane (3 × 10 mL), and the dichloromethane phase was combined, rinsed with NaCl solution (10 mL), dried over Na_2SO_4, filtered, solvent-removed and finally fractionated by silica gel CC (light petroleum/EtOAc, 100:1 to 20:1) to afford **4** (19.2 mg, 96.8% yield).

*Methyl (E)-3-(4-hydroxy-3-methylbut-2-en-*1-yl*)-1,4-dioxo-1,4-dihydronaphthalene-2-carboxylate (**3**).* Under the protection of N_2, compound **4** (20.0 mg, 0.078 mmol, 1.0 equiv.) and methallyl alcohol (13.1 μL, 0.156 mmol, 2.0 equiv.) in 2.0 mL toluene were put into a Schlenk pressure tube, followed by the addition of Hoveyda-Grubbs catalyst (II) (9.7 mg, 0.016 mmol, 0.2 equiv.). The reaction solution was heated to 80 °C and allowed to stand for 8 h. The product **3** (5.8 mg, 24.8% yield) was isolated over silica gel (light petroleum/EtOAc, 10:1 to 5:1). ^{1}H NMR (500 MHz, chloroform-*d*) δ 8.13−8.06 (m, 2H), 7.79−7.74 (m, 2H), 5.40 (m), 4.00 (d, J = 1.2 Hz, 2H), 3.95 (s, 3H), 3.40−3.34 (m, 2H), 1.79 (s, 3H) ppm. ^{13}C NMR (125 MHz, chloroform-*d*) δ 184.4, 182.1, 165.1, 145.8, 138.6, 134.4, 131.8, 131.4, 126.9, 126.6, 119.6, 68.4, 53.0, 27.0, 14.0 ppm. HR-ESIMS *m/z* $[M+Na]^+$ 323.0890 (calcd for $C_{17}H_{16}O_5Na^+$, 323.0891).

*(±)-Nonin A (**2**).* To a solution of intermediate **3** (5.0 mg, 0.017 mmol, 1.0 equiv.) in dichloromethane (2.0 mL) at zero degree was added triethylamine (2.8 μL, 0.02 mmol, 1.2 equiv.), and the reaction was warmed to r.t. and stirred for 48 h until the finish. The product **2** (3.91 mg, 76.6% yield) was acquired from purification by silica gel CC (light petroleum/EtOAc, 5:1 to 3.3:1). ^{1}H NMR (500 MHz, chloroform-*d*) δ 12.19 (s), 8.38 (d, J = 8.1 Hz), 8.15 (d, J = 8.1 Hz), 7.63 (ddd, J = 8.2, 6.8, 1.3 Hz), 7.53 (ddd, J = 8.2, 6.8, 1.3 Hz), 7.27 (d, J = 10.1 Hz), 5.69 (d, J = 10.1 Hz), 4.03 (s, 2H), 3.81 (d, J = 11.7 Hz), 3.73 (d, J = 11.7 Hz), 1.43 (s, 3H) ppm. ^{13}C NMR (125 MHz, chloroform-*d*) δ 172.5, 157.0, 140.9, 129.8, 128.8, 126.7, 125.4, 125.3, 124.8, 124.4, 121.7, 112.6, 102.3, 78.1, 68.1, 52.5, 21.6 ppm.

*(±)-MPE (**1**).* To a solution of (±)-nonin A (**2**, 23.1 mg, 0.077 mmol, 1.0 equiv.) in dichloromethane (3.0 mL) at 0 °C was added (diacetoxyiodo)benzene (54.8 mg, 0.17 mmol, 2.2 equiv.). The reaction mixture was stirred for another 2 h until the end, solvent-removed and finally fractionated by silica gel CC (light

cytometry. Bars represent mean ± SD of three independent experiments. (D) MDA-MB231 cells were treated with indicated concentrations of (+)/(−)-MPE and the expressions of cleaved-PARP and cleaved-caspase 3 were detected by Western blotting assay with the indicated antibodies. Protein expressions were quantitated by densitometry and normalized against that of β-actin. Bars represent mean ± SD of three independent experiments. (E, F) MDA-MB231 and MCF-7 cells were treated with indicated concentrations of (+)/(−)-MPE and co-incubated for 24 h. Cell population distribution was determined following PI staining and further analyzed by flow cytometry. Bars represent mean ± SD of three independent experiments. (G, H) MDA-MB231 and MCF-7 cells were treated with indicated concentrations of (+)/(−)-MPE and the expression of cell cycle-related proteins were detected by Western blotting assay with the indicated antibodies. Protein expressions were quantitated by densitometry and normalized against that of β-actin. Bars represent mean ± SD of three independent experiments. ns, no significant difference, $^*P < 0.05$, $^{**}P < 0.01$, $^{***}P < 0.001$ *versus* the control group.

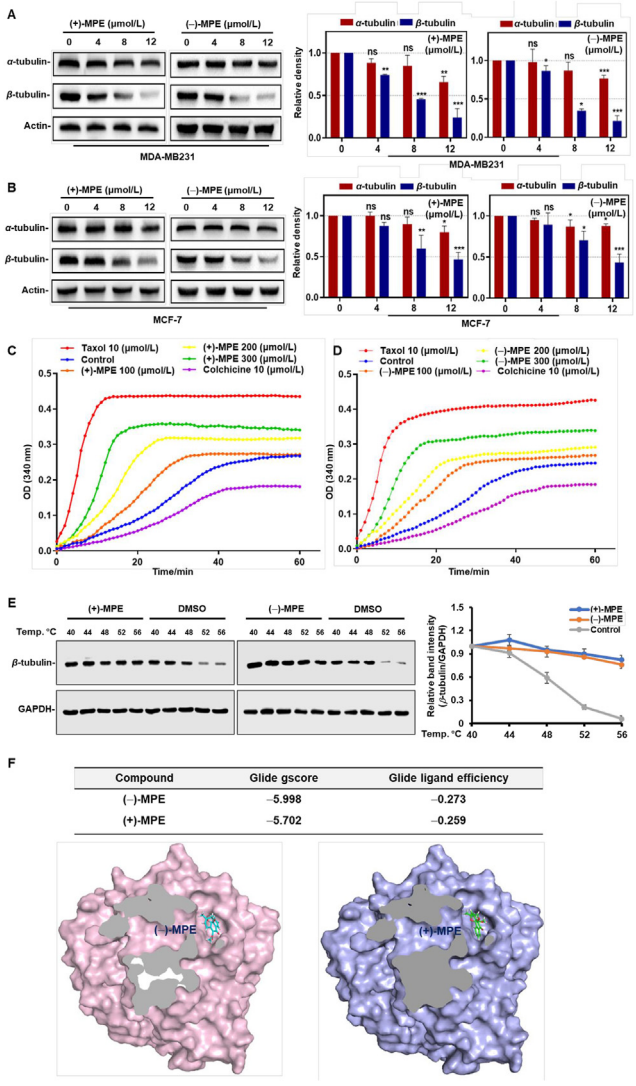

Figure 4 (+)/(−)-MPE inhibit the depolymerization of tubulin. (A, B) MDA-MB231 and MCF-7 cells were treated with indicated concentrations of (+)/(−)-MPE and the expressions of α and β-tubulin were detected by Western blotting assay with the indicated antibodies. Protein expressions were quantitated by densitometry and normalized against that of β-actin. Bars represent mean ± SD of three independent experiments. ns, no significant difference, $^{*}P < 0.05$, $^{**}P < 0.01$, $^{***}P < 0.001$ *versus* the control group. (C, D) *In vitro* tubulin polymerization assay was performed. Tubulin was exposed to DMSO, colchicine (10 μmol/L), paclitaxel (10 μmol/L) or the indicated concentrations of (+)/(−)-MPE. GTP was added to initiate the reaction. The tubulin polymerization rate was monitored for 60 min at 37 °C and the absorbance at 340 nm was measured. (E) MDA-MB231 cells were lysed using liquid nitrogen and three repeated cycles of freeze-thaw, and the cell lysate was treated with (+)/(−)-MPE (12 μmol/L) or DMSO for 30 min at r.t. The cell suspension was heated for 3 min to 40, 44, 48, 52 and 56 °C, cooled at 25 °C for 3 min, and then centrifuged at 20,000 ×*g* for 30 min. Finally, the supernatant was collected for Western blot analysis. (F) Cut-away view of the ligand-binding pocket at the laulimalide site in the docking complexes of (+)/(−)-MPE with β-tubulin.

petroleum/EtOAc 3:1) to yield (±)-MPE (**1**, 16.7 mg, 72.8% yield). ^{1}H NMR (600 MHz, chloroform-*d*) δ 8.10 (dd, J = 7.9, 1.2 Hz), 7.75 (dd, J = 7.9, 1.2 Hz), 7.67 (ddd, J = 7.9, 7.3, 1.3 Hz), 7.56 (ddd, J = 7.9, 7.3, 1.3 Hz), 6.62 (d, J = 9.5 Hz), 6.59 d, J = 9.5 Hz), 3.95 (d, J = 6.6 Hz), 3.91 (s, 3H), 3.84 (d, J = 6.6 Hz), 1.71 (s, 3H) ppm. ^{13}C NMR (150 MHz, chloroform-*d*) δ 181.1, 165.3, 146.5, 143.5, 137.0, 133.7, 131.1, 130.3, 126.6, 126.5, 126.2, 123.6, 98.9, 81.0, 74.0, 52.7, 19.6 ppm.

4.2. *Biology*

4.2.1. *Cell lines and reagents*

See Supporting Information.

4.2.2. *Animal experiments*

Female BALB/c mice, aged between 6 and 8 weeks, were procured from the Institute of Laboratory Animal Science at the Chinese Academy of Medical Sciences in Beijing, China. All procedures involving these animals were in strict compliance with the guidelines laid out by the Institutional Animal Care and aligned with Qingdao University's animal research protocols. Moreover, the Ethics Committee of Qingdao University's Medical College granted their endorsement for these procedures. The mice were divided into two groups, each with 5 members. The test group was given an IP injection of (±)-MPE at a rate of 5 mg/kg/day, while the control group was administered PBS injections every other day. Weights of the mice were diligently recorded every week. On completing the 28th day, the mice were euthanized in a humane manner, their vital organs were swiftly retrieved, preserved, and subsequently embedded in paraffin, ready for H&E staining.

Another independent experiment was performed to evaluate the potential side effects of (±)-MPE using a set of healthy mice, segmented into groups of 5 each.

4.2.3. *Cell viability assay*

The cell viability assay was conducted based on previously established methods[29]. Briefly, MDA-MB231 and MCF-7 cells (5×10^3 cells/well) were placed in 96-well plates. After a 24-h period, these cells underwent treatment with varying concentrations of the compounds under investigation. 24 h later, the MTT method was employed to evaluate cell viability, with absorbance readings taken at 490 nm. This procedure was replicated in three separate experiments, each performed in triplicate.

4.2.4. *Colony formation assay*

The colony formation assay was conducted following a previously referenced procedure[30]. Briefly, MDA-MB231 and MCF-7 cells were distributed in a 6-well plate. 12 h post-seeding, the cells were treated with the designated concentrations of (+)/(−)-MPE. The medium was refreshed every other day, and the cells were cultivated for a duration of 1−2 weeks. At the end of this period, colonies were fixed using 4% paraformaldehyde, stained with 0.1% crystal violet, and subsequently counted manually.

4.2.5. *Soft agar colony formation assay*

Agar solutions of 0.7% and 1.2% concentrations were formulated and then sterilized through autoclaving. Next, they were mixed

with an equivalent volume of cell culture medium, which was doubly fortified with FBS and penicillin/streptomycin. The 1.2% agar was dispensed into a 6-well plate and set aside to solidify. Simultaneously, the processed tumor cells were gathered, amalgamated with the 0.7% agar, and then spread over the set 1.2% agar. These cells were maintained in culture for 14 days, receiving fresh culture medium every three days. Upon completion of the culture period, the cells were dyed with crystal violet. Illustrative images were then taken using an Olympus BX53 microscope, based in Tokyo, Japan.

4.2.6. *Cell cycle analysis*

MDA-MB231 and MCF-7 cells were placed in 6 cm dishes and exposed to designated concentrations of (+)/(−)-MPE for 24 h before undergoing trypsinization. Post-centrifugation, these cells were secured and preserved in ice-cold 70% ethanol, with a resting period at 4 °C for 24 h. They were then thoroughly washed with PBS multiple times. Subsequently, these fixed cells were immersed in PBS supplemented with RNase and PI solution, and then incubated for 30 min at 37 °C, away from light exposure. The cell cycle progression was assessed using a flow cytometer provided by BD Biosciences in Pasadena, CA, USA. This experimental process was systematically conducted in three separate trials, with each iteration done in triplicate.

4.2.7. *Cell death analysis*

Apoptosis evaluations were performed utilizing the Annexin V-FITC/propidium iodide (PI) assay, following prior protocols[31]. Briefly, MDA-MB231 and MCF-7 cells underwent treatment with increasing concentrations of (+)/(−)-MPE for 24 h. After this period, the cells were stained with the Annexin V-FITC/PI apoptosis detection solution and subsequently analyzed *via* a FACS Aria flow cytometer provided by BD Biosciences.

4.2.8. *Wound healing assay*

MDA-MB231 and MCF-7 cells were cultured in 6-well plates until they reached complete confluence. A 'scratch' or 'wound' was subsequently made with a sterile 100 μL pipette tip. After this, the cells were either treated with a fresh serum-free medium or one enriched with varying concentrations of (+)/(−)-MPE. After a 24-h migration window, the cells were fixed using 4% paraformaldehyde. Observations of the migration activity were captured with an inverted IX-71 microscope from Olympus, Tokyo, Japan. The migrated cells were then quantified by hand.

4.2.9. *Cell invasion assay*

MDA-MB231 and MCF-7 cells were first subjected to overnight fasting and then reconstituted in 100 μL of serum-free medium. These cells, at a concentration of 5×10^4 cells/well, were introduced into Transwell chambers that had been pre-treated with a 1 mg/mL matrigel layer. Specified concentrations of (+)/(−)-MPE were then administered to both compartments of the Transwell. After a 12-h incubation, cells that invaded and settled on the undersurface were stabilized with 4% paraformaldehyde and highlighted with a 0.1% crystal violet stain. Cells that remained non-invasive and were situated on the upper surface of the Transwell were meticulously cleared using cotton swabs. The cells that had invaded were visualized and captured with an inverted IX-71 microscope by Olympus, Tokyo, Japan, and then counted manually.

4.2.10. *Western blotting experiment*

Cells were harvested with RIPA buffer containing 150 mmol/L sodium chloride, 1% Triton X-100, 0.5% sodium deoxycholate, 0.1% SDS, 50 mmol/L Tris, and a combination of protease and phosphatase inhibitors. The concentration of the resulting soluble protein lysates was determined using the BCA protein assay kit (Pierce, Rockford, IL, USA, Cat# 23225). Uniform quantities of total or nuclear protein, ranging from 20 to 120 μg, were separated on 8%−12% SDS-PAGE and then relayed onto polyvinylidene difluoride nitrocellulose sheets (Millipore, Billerica, MA, USA). These sheets were subsequently blocked using 5% BSA, incubated with specific primary antibodies, and later introduced to HRP-affixed anti-rabbit or anti-mouse secondary antibodies (Sigma, St. Louis, MO, USA). After rinsing three times with TBST, the prominent bands were visualized using the chemiluminescence Western blot detection reagent (ECL kit; Cat# ab65623; Abcam) and imaged on auto-radiographic film. The entire process was replicated three times, each time with triplicate samples.

4.2.11. *In vitro tubulin polymerization assay*

The tubulin polymerization assay was performed *in vitro*, using the recommended guidelines from Cytoskeleton (Cat# BK006P). Various concentrations of (+)/(−)-MPE (100, 200, 300 μmol/L) were amalgamated with 10 μmol/L of paclitaxel, 10 μmol/L of colchicine, and a DMSO control. This blend was combined with tubulin protein in a 100 μL reaction buffer that consisted of 80 mmol/L PIPES, 2.0 mmol/L $MgCl_2$, 0.5 mmol/L EGTA, 15% glycerol, and 1 mmol/L GTP, all set to a pH of 6.9. Following this, the mixture underwent incubation at 37 °C, with its development observed using a microplate reader (Tecan Spark 10M, Tecan, Austria). The absorbance at 340 nm was recorded at intervals of 60 s over an hour's time. It is important to note that paclitaxel and colchicine served as reference positive indicators.

4.2.12. *Cellular thermal shift assay (CETSA)*

The interaction of (+)/(−)-MPE with β-tubulin in intact cells was analyzed by CETSA developed by Molina et al.[32]. Briefly, MDA-MB231 cells were lysed using liquid nitrogen and three repeated cycles of freeze-thaw, and then the cell lysate was treated with (+)/(−)-MPE (12 μmol/L) or DMSO for 30 min at room temperature (r.t.). The cell suspension was subsequently heated for 3 min to 40, 44, 48, 52 and 56 °C, cooled at 25 °C for 3 min, and centrifuged at 20,000 ×*g* for 30 min. Lastly, the supernatant was collected for Western blot analysis.

4.2.13. *Molecular docking of (+)/(−)-MPE to the taxane site and laulimalide site*

Molecular docking procedures were carried out using the Glide tool within the Maestro software suite (Schrödinger LLC, New York, USA, 2015). As both taxane site and laulimalide site are located on β-tubulin, only coordinates of this subunit and the corresponding small molecule were retained for the docking work, and the initial model for docking into the taxane site was built using the complex crystal structure of (+)-discodermolide with tubulin (PDB ID: 5LXT)[33]. The first phase involved prepping the

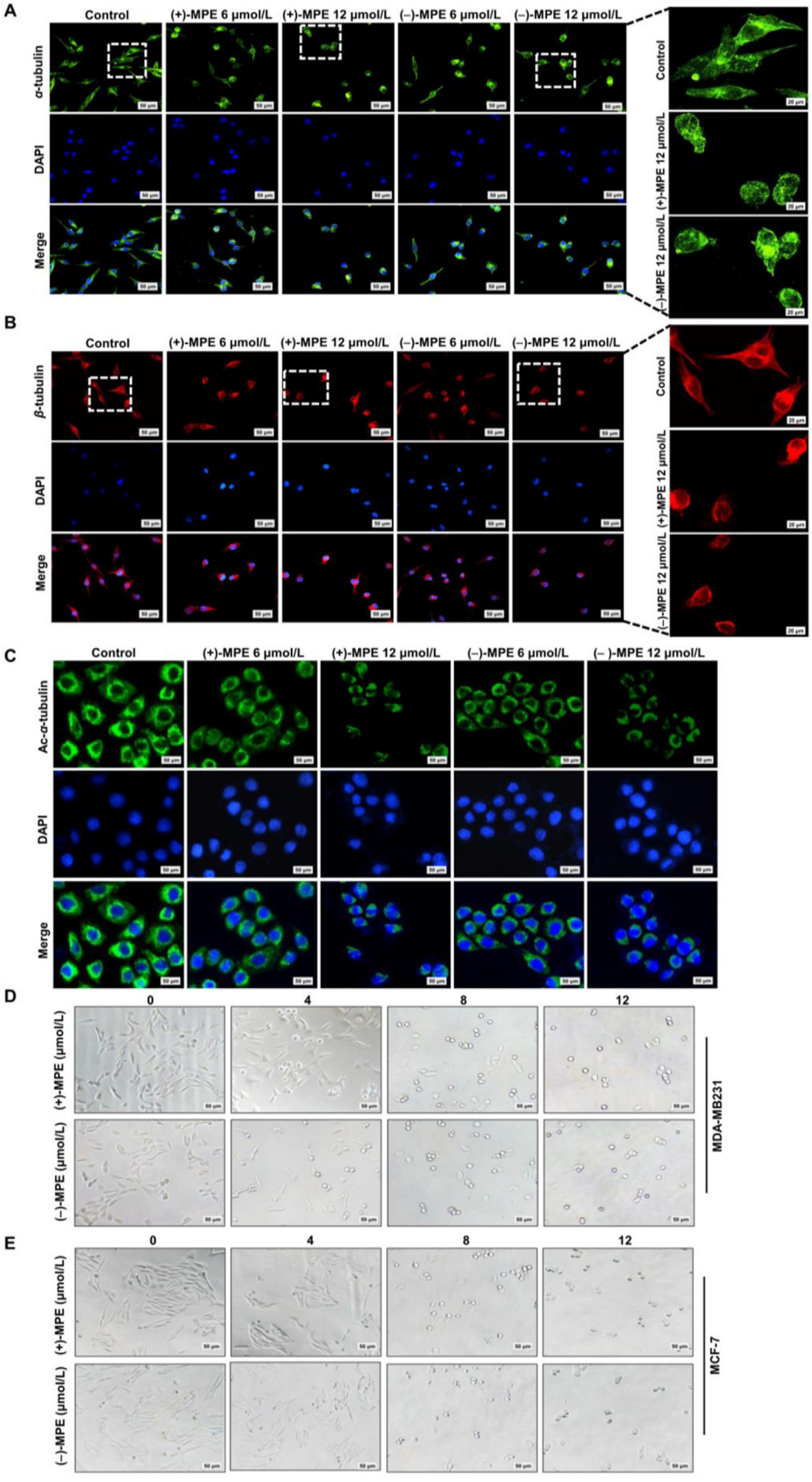

Figure 5 (+)/(−)-MPE induce cell death by disrupting the dynamic equilibrium of tubulin assembly. (A, B) MDA-MB231 cells were treated with indicated concentrations of (+)/(−)-MPE for 24 h. Tubulin was stained with anti-α-tubulin (green) and anti-β-tubulin (red) antibodies, while

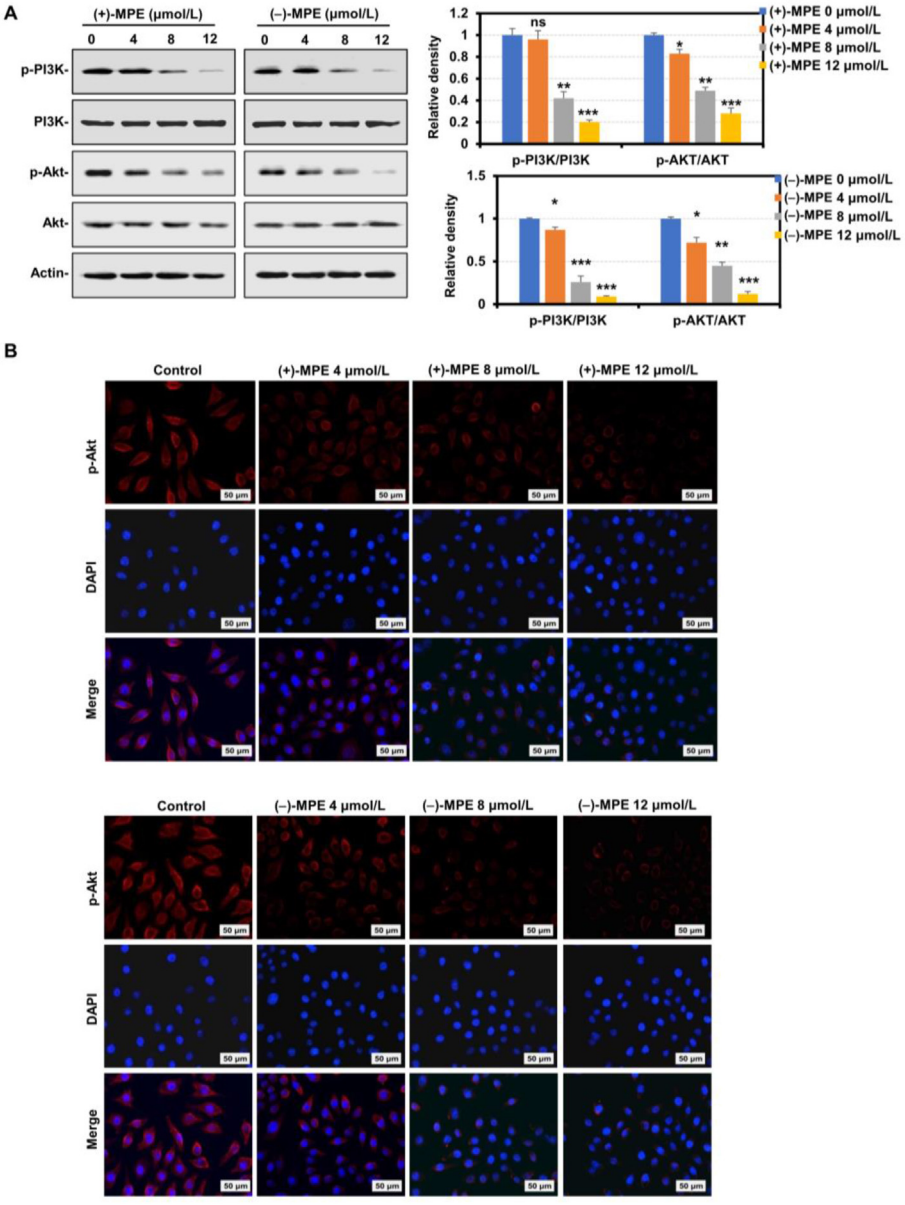

Figure 6 (+)/(−)-MPE regulate microtubule stability *via* inhibiting PI3K/Akt signaling pathway. (A) MDA-MB231 cells were treated with indicated concentrations of (+)/(−)-MPE, and the expressions of key proteins of PI3K/Akt signaling were detected by Western blotting assay with the indicated antibodies. Protein expressions were quantitated by densitometry and normalized against that of β-actin. Bars represent mean ± SD of three independent experiments. ns, no significant difference, $^{*}P < 0.05$, $^{**}P < 0.01$, $^{***}P < 0.001$ *versus* the control group. (B) MDA-MB231 cells were treated with indicated concentrations of (+)/(−)-MPE for 24 h, and cells were stained for p-Akt (red) and the nucleus (blue) was stained with DAPI by immunofluorescence assay.

composite structure *via* the Protein Preparation Wizard, which involves hydrogenation, charge assignment and removal of water molecules distant from the binding pocket, followed by a restrained energy optimization. Subsequently, a grid file was generated with the amino acid residues within a 15 Å radius around the small molecule serving as the docking site. Next, (+)/(−)-MPE were prepared with Ligprep program (LigPrep, version 2.3) using the default parameters. Finally, the prepared small molecules were docked into the grid file using XP mode for scoring predictions.

the nucleus (blue) was stained with DAPI. The boxed areas were magnified to show changes of the microtubule network in (+)/(−)-MPE-treated cells by immunofluorescence assay. (C) MDA-MB231 cells were treated with indicated concentrations of (+)/(−)-MPE for 24 h, and the cells were then stained for Ac-α-tubulin (green) and the nucleus (blue) was stained with DAPI by immunofluorescence assay. (D, E) MDA-MB231 and MCF-7 cells were treated with indicated concentrations of (+)/(−)MPE for 24 h, and then the morphological changes of cells were photographed by microscope.

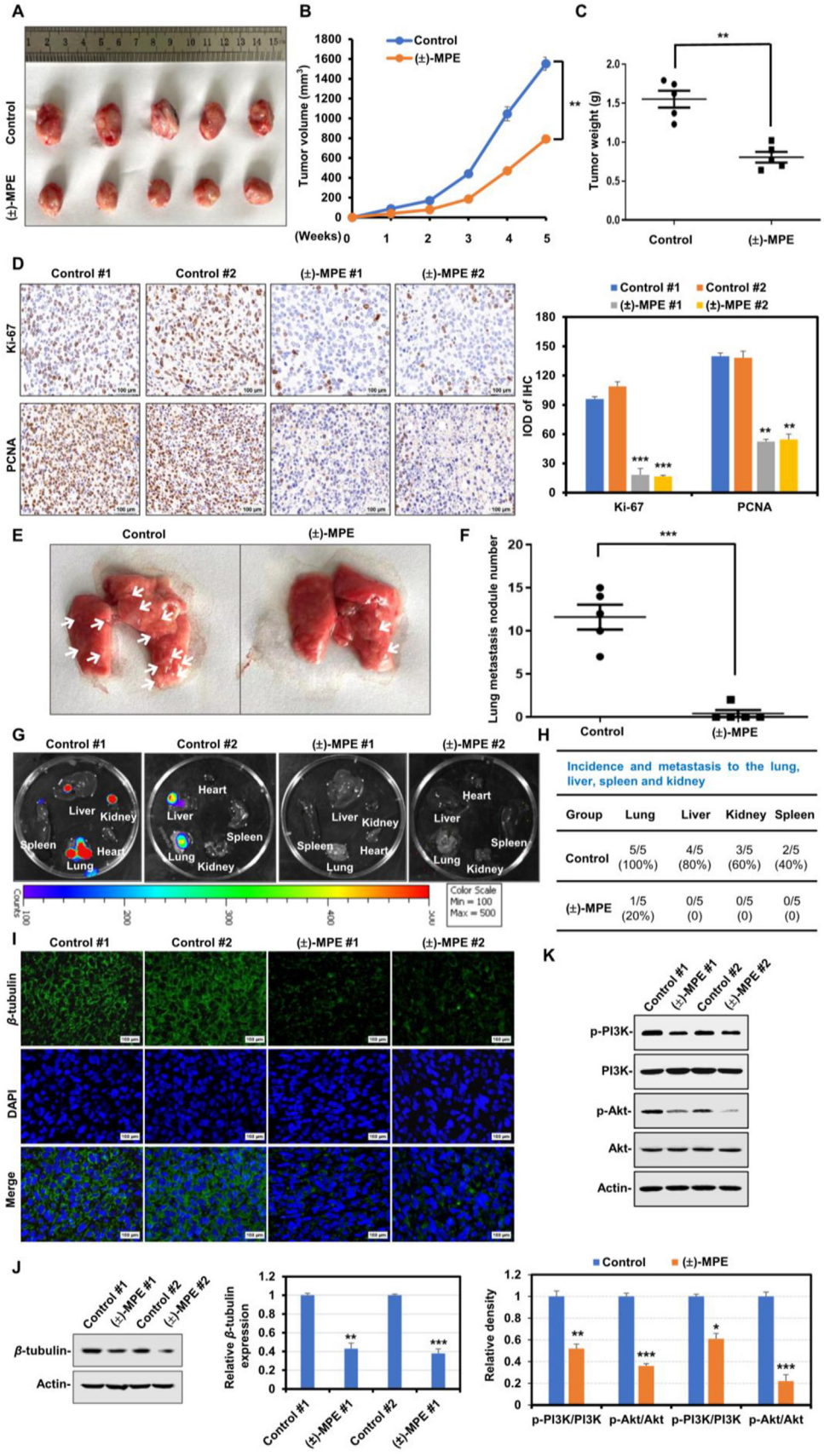

Figure 7 (±)-MPE inhibits tumor growth and metastasis in a preclinical animal model. (A) Photographs of the primary tumors from mice administrated with PBS (control) or (±)-MPE for 28 days. (B) Primary tumor volume was measured each week. (C) Primary tumor weight in each

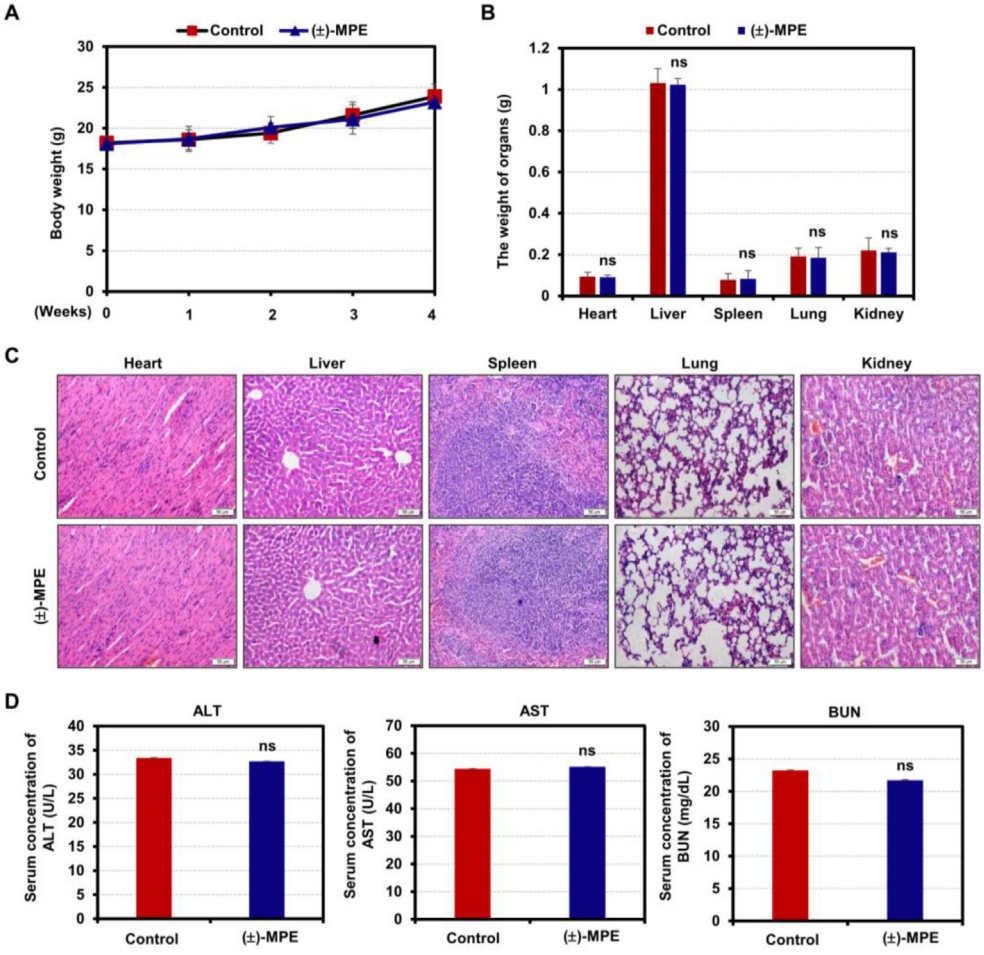

Figure 8 (±)-MPE shows no systematic toxicity on mice. (A) (±)-MPE or PBS (control) were administered to normal female BALB/c mice at 5 mg/kg once every two days for 28 days, and the mice's body weight was monitored once a week. Each treatment group consisted of five mice. (B) Major organs were removed from the executed mice after the last drug treatment and the weight was measured. (C) Major organs of randomly selected mice from different groups were stained with H&E (scale bar 50 μm) and observed under an inverted microscope (IX-71, Olympus, Tokyo, Japan). (D) Blood samples were collected 24 h after the last treatment and the serum concentrations of ALT, AST and BUN were measured using Fuji DRI-CHEM 7000i (Fujifilm, Japan).

Similarly, the molecular docking of (+)/(−)-MPE into the laulimalide site was conducted with the complex crystal structure of laulimalide with tubulin (PDB ID: 4O4H)[34].

4.2.14. *Immunofluorescence staining*

Immunofluorescence staining was executed as previously described[29]. Briefly, cells were fixed using 4% formaldehyde for a span of 10 min. They were then subjected to the primary antibody incubation for either 2 h at ambient temperature or overnight at 4 °C. This step was followed by a 2-h incubation with the secondary antibodies that were fluorescently labeled: Alexa Fluor 488-conjugated IgG (Cat#: A11034) and Alexa Fluor 568-conjugated IgG (Cat#: A20341), both sourced from Invitrogen. The fluorescence emanating from these cells was then visualized and documented using a DM1000 fluorescence microscope by Leica, Germany.

4.2.15. *Hematoxylin-eosin (H&E) staining*

Following the experiments, organs from mice, including hearts and livers, were swiftly gathered and fixed in 4% paraformaldehyde for an overnight period. These were then set in paraffin. Afterward, 4 μm thick sections were produced and

group was measured after the experiment. (D) Primary tumors were fixed and paraffin embedded. Five-micrometer (5 μm) sections were analyzed by IHC staining using anti-Ki67 and anti-PCNA antibodies. Scale bar, 100 μm. The IHC results were analyzed by Image-Pro Plus 6.0 ($n = 5$ fields of view). (E, F) Metastatic lung nodules were visualized and then counted manually, and the differences were evaluated with Student *t*-test. (G, H) *Ex vivo* bioluminescence images were obtained for randomly selected mice in each group to check the effect of (±)-MPE against distant metastasis, and the metastasis incidence to distant organs was quantified. (I) Primary tumor sections were stained for β-tubulin (green) and nuclei were counterstained with DAPI (blue). Scale bar, 50 μm. (J, K) Primary tumors were lysed and applied to immunoblotting analysis using the indicated antibodies, with actin as a loading control. Bars represent mean ± SD of three independent experiments. $^{*}P < 0.05$, $^{**}P < 0.01$, $^{***}P < 0.001$ *versus* the control group.

stained using H&E. Images exemplifying these sections were taken with a Leica DM4000b microscope, manufactured in Germany.

4.2.16. *Immunohistochemical (IHC) staining*

IHC staining was conducted following methods detailed in previous publications[29,35]. The staining involved the use of antibodies specific to PCNA and Ki67. Representative images were then taken using a German-made Leica DM4000b microscope.

4.2.17. *Preliminary evaluation of pharmacokinetics and bioavailability*

Briefly, eighteen 8-week old female BALB/c mice were randomly divided into two groups (nine in each group) that received intravenous (iv) and oral (*per os*, *po*) administrations with 10 and 30 mg/kg (±)-MPE, respectively. The nine mice in the two respective groups were further randomly divided into three subgroups, with three animals in each group. A cross-collection method was employed to ensure that there were three parallel blood samples at each collecting time point in each dose group. Blood samples were collected from the cheek vein into EDTA-treated anticoagulation tubes at 1/12, 1/4, 1/2, 1, 2, 4, 8, 24 and 48 h after drug administration. Then the whole blood samples were centrifuged at 6000×*g* for 10 min at 4 °C. The obtained plasma was stored by freezing at −80 °C for further LC−MS/MS detection. The pharmacokinetic parameters of (±)-MPE were calculated based on the non-compartmental model, by using blood drug concentration data.

4.2.18. *Statistical analyses*

Every experiment incorporated both control and test groups and took place on at least three distinct instances. The results are displayed as the mean ± SD, based on a minimum of three separate experiments. The notation "*n*" signifies the number of biological replicates, as detailed in the figure legends. When contrasting two groups, a Student's *t*-test was used, considering $P < 0.05$ as significant unless otherwise mentioned. Each experimental procedure was carried out no less than three times.

Acknowledgments

This project was financially supported by the National Natural Science Foundation of China (No. 82073729, 22225105).

Author contributions

Conceptualization, Hua Zhang; Methodology, Hua Zhang, Peipei Shan, Shuanhu Gao; Investigation: Peipei Shan, Tao Ye, Ying-De Tang, Hui Song, Chao Wang, Pei-Wen Su; Formal analysis, Peipei Shan, Tao Ye, Ying-De Tang, Feifei Yang, Shi-Lei Zhang, Hua Zhang; Data curation, Peipei Shan, Hua Zhang; Writing (original draft), Peipei Shan and Hua Zhang; Writing (review and editing), Peipei Shan and Hua Zhang; Supervision, Hua Zhang, Shuanhu Gao; Project administration, Hua Zhang; Funding acquisition, Hua Zhang and Shuanhu Gao.

Conflicts of interest

The authors declare that they have no known competing financial interests or personal relationships that could have appeared to influence the work reported in this paper.

Appendix A. Supporting information

Supporting data to this article can be found online at https://doi.org/10.1016/j.apsb.2024.02.012.

References

1. Baskar R, Lee KA, Yeo R, Yeoh KW. Cancer and radiation therapy: current advances and future directions. *Int J Med Sci* 2012;**9**:193−9.
2. Nagai H, Kim YH. Cancer prevention from the perspective of global cancer burden patterns. *J Thorac Dis* 2017;**9**:448−51.
3. Nakashima J, Ueno M, Nakamura K, Tachibana M, Baba S, Deguchi N, et al. Differential diagnosis of primary benign and malignant retroperitoneal tumors. *Int J Urol* 1997;**4**:441−6.
4. Jordan MA, Wilson L. Microtubules as a target for anticancer drugs. *Nat Rev Cancer* 2004;**4**:253−65.
5. Steinmetz MO, Prota AE. Microtubule-targeting agents: strategies to hijack the cytoskeleton. *Trends Cell Biol* 2018;**28**:776−92.
6. Vicente JJ, Wordeman L. The quantification and regulation of microtubule dynamics in the mitotic spindle. *Curr Opin Cell Biol* 2019;**60**:36−43.
7. Arnst KE, Banerjee S, Chen H, Deng SS, Hwang DJ, Li W, et al. Current advances of tubulin inhibitors as dual acting small molecules for cancer therapy. *Med Res Rev* 2019;**39**:1398−426.
8. van Vuuren RJ, Visagie MH, Theron AE, Joubert AM. Antimitotic drugs in the treatment of cancer. *Cancer Chemother Pharmacol* 2015;**76**:1101−12.
9. Zhao Y, Mu X, Du GH. Microtubule-stabilizing agents: new drug discovery and cancer therapy. *Pharmacol Therapeut* 2016;**162**:134−43.
10. Chang LC, Yu YL, Liu CY, Cheng YY, Chou RH, Hsieh MT, et al. The newly synthesized 2-arylnaphthyridin-4-one, CSC-3436, induces apoptosis of non-small cell lung cancer cells by inhibiting tubulin dynamics and activating CDK1. *Cancer Chemother Pharmacol* 2015;**75**:1303−15.
11. Foley EA, Kapoor TM. Microtubule attachment and spindle assembly checkpoint signalling at the kinetochore. *Nat Rev Mol Cell Biol* 2013;**14**:25−37.
12. Ghawanmeh AA, Chong KF, Sarkar SM, Bakar MA, Othaman R, Khalid RM. Colchicine prodrugs and codrugs: chemistry and bioactivities. *Eur J Med Chem* 2018;**144**:229−42.
13. Li L, Jiang S, Li X, Liu Y, Su J, Chen J. Recent advances in trimethoxyphenyl (TMP) based tubulin inhibitors targeting the colchicine binding site. *Eur J Med Chem* 2018;**151**:482−94.
14. Davies MA. The role of the PI3K-AKT pathway in melanoma. *Cancer J* 2012;**18**:142−7.
15. Mundi PS, Sachdev J, McCourt C, Kalinsky K. AKT in cancer: new molecular insights and advances in drug development. *Br J Clin Pharmacol* 2016;**82**:943−56.
16. Wu Z, Yu X, Zhang S, He Y, Guo W. The role of PI3K/AKT signaling pathway in gallbladder carcinoma. *Am J Transl Res* 2022;**14**:4426−42.
17. Su Y, Wan D, Song W. Dryofragin inhibits the migration and invasion of human osteosarcoma U2OS cells by suppressing MMP-2/9 and elevating TIMP-1/2 through PI3K/AKT and p38 MAPK signaling pathways. *Anti Cancer Drugs* 2016;**27**:660−8.
18. Paz-Ares L, Blanco-Aparicio C, Garcia-Carbonero R, Carnero A. Inhibiting PI3K as a therapeutic strategy against cancer. *Clin Transl Oncol* 2009;**11**:572−9.
19. Vivanco I, Sawyers CL. The phosphatidylinositol 3-kinase AKT pathway in human cancer. *Nat Rev Cancer* 2002;**2**:489−501.
20. Fujiwara Y, Hosokawa Y, Watanabe K, Tanimura S, Ozaki K, Kohno M. Blockade of the phosphatidylinositol-3-kinase-Akt signaling pathway enhances the induction of apoptosis by microtubule-destabilizing agents in tumor cells in which the pathway is constitutively activated. *Mol Cancer Therapeut* 2007;**6**:1133−42.

21. Onishi K, Higuchi M, Asakura T, Masuyama N, Gotoh Y. The PI3K-Akt pathway promotes microtubule stabilization in migrating fibroblasts. *Gene Cell* 2007;**12**:535−46.
22. Yu JH, Zhai HJ, Yu ZP, Zhang QQ, Ge YX, Zhang YY, et al. Methyl 2-naphthoates from a traditional Chinese herb *Morinda officinalis* var. officinalis. *Tetrahedron* 2019;**75**:3793−801.
23. Sastry MN, Claessens S, Habonimana P, De Kimpe N. Synthesis of the natural products 3-hydroxymollugin and 3-methoxymollugin. *J Org Chem* 2010;**75**:2274−80.
24. Connon SJ, Blechert S. Recent developments in olefin cross-metathesis. *Angew Chem Int Ed Engl* 2003;**42**:1900−23.
25. Kang Y, Massague J. Epithelial-mesenchymal transitions: twist in development and metastasis. *Cell* 2004;**118**:277−9.
26. Yang J, Yu Y, Li Y, Yan W, Ye H, Niu L, et al. Cevipabulin−tubulin complex reveals a novel agent binding site on alpha-tubulin with tubulin degradation effect. *Sci Adv* 2021;**7**:eabg4168.
27. Shuai W, Wang G, Zhang Y, Bu F, Zhang S, Miller DD, et al. Recent progress on tubulin inhibitors with dual targeting capabilities for cancer therapy. *J Med Chem* 2021;**64**:7963−90.
28. Eshun-Wilson L, Zhang R, Portran D, Nachury MV, Toso DB, Lohr T, et al. Effects of alpha-tubulin acetylation on microtubule structure and stability. *Proc Natl Acad Sci U S A* 2019;**116**:10366−71.
29. Shan P, Yang F, Qi H, Hu Y, Zhu S, Sun Z, et al. Alteration of MDM2 by the small molecule YF438 exerts antitumor effects in triple-negative breast cancer. *Cancer Res* 2021;**81**:4027−40.
30. Shan P, Wang C, Chen H, Yu J, Zhang H. Inonotsutriol E from Inonotus obliquus exhibits promising anti breast cancer activity *via* regulating the JAK2/STAT3 signaling pathway. *Bioorg Chem* 2023;**139**:106741.
31. Shan P, Yang F, Yu J, Wang L, Qu Y, Qiu H, et al. A novel histone deacetylase inhibitor exerts promising anti-breast cancer activity *via* triggering AIFM1-dependent programmed necrosis. *Cancer Commun* 2022;**42**:1207−11.
32. Martinez Molina D, Jafari R, Ignatushchenko M, Seki T, Larsson EA, Dan C, et al. Monitoring drug target engagement in cells and tissues using the cellular thermal shift assay. *Science* 2013;**341**:84−7.
33. Prota AE, Bargsten K, Redondo-Horcajo M, Smith 3rd AB, Yang CH, McDaid HM, et al. Structural basis of microtubule stabilization by discodermolide. *Chembiochem* 2017;**18**:905−9.
34. Prota AE, Bargsten K, Northcote PT, Marsh M, Altmann KH, Miller JH, et al. Structural basis of microtubule stabilization by laulimalide and peloruside A. *Angew Chem Int Ed* 2014;**53**:1621−5.
35. Shan PP, Fan GJ, Sun LH, Liu JQ, Wang WF, Hu C, et al. SIRT1 functions as a negative regulator of eukaryotic poly(A)RNA transport. *Curr Biol* 2017;**27**:2271−2284.e5.
36. Yu JH, Yu ZP, Capon RJ, Zhang H. Natural enantiomers: occurrence, biogenesis and biological properties. *Molecules* 2022;**27**:1279.
37. Steeg PS. Perspective: the right trials. *Nature* 2012;**485**:S58−9.
38. Akhshi TK, Wernike D, Piekny A. Microtubules and actin crosstalk in cell migration and division. *Cytoskeleton (Hoboken)* 2014;**71**:1−23.
39. Romagnoli R, Salvador MK, Ortega SS, Baraldi PG, Oliva P, Baraldi S, et al. 2-Alkoxycarbonyl-3-arylamino-5-substituted thiophenes as a novel class of antimicrotubule agents: design, synthesis, cell growth and tubulin polymerization inhibition. *Eur J Med Chem* 2018;**143**:683−98.
40. Li F, Liu Z, Sun H, Chun Li, Wang W, Ye L, et al. PCC0208017, a novel small-molecule inhibitor of MARK3/MARK4, suppresses glioma progression *in vitro* and *in vivo*. *Acta Pharm Sin B* 2020;**10**:289−300.
41. Banerjee S, Arnst KE, Wang YX, Kumar G, Deng SS, Yang L, et al. Heterocyclic-fused pyrimidines as novel tubulin polymerization inhibitors targeting the colchicine binding site: structural basis and antitumor efficacy. *J Med Chem* 2018;**61**:1704−18.
42. Borisy G, Heald R, Howard J, Janke C, Musacchio A, Nogales E. Microtubules: 50 years on from the discovery of tubulin. *Nat Rev Mol Cell Biol* 2016;**17**:322−8.
43. Perez EA. Microtubule inhibitors: differentiating tubulin-inhibiting agents based on mechanisms of action, clinical activity, and resistance. *Mol Cancer Therapeut* 2009;**8**:2086−95.
44. Kavallaris M. Microtubules and resistance to tubulin-binding agents. *Nat Rev Cancer* 2010;**10**:194−204.
45. Bumbaca B, Li W. Taxane resistance in castration-resistant prostate cancer: mechanisms and therapeutic strategies. *Acta Pharm Sin B* 2018;**8**:518−29.